

ENERGY STABLE RUNGE-KUTTA DISCONTINUOUS GALERKIN SCHEMES FOR FOURTH ORDER GRADIENT FLOWS

HAILIANG LIU[†] AND PEIMENG YIN[§]

ABSTRACT. We present unconditionally energy stable Runge-Kutta (RK) discontinuous Galerkin (DG) schemes for solving a class of fourth order gradient flows. Our algorithm is geared toward arbitrarily high order approximations in both space and time, while energy dissipation remains preserved without imposing any restriction on time steps and meshes. We achieve this in two steps. First, taking advantage of the penalty free DG method introduced by Liu and Yin [J Sci. Comput. 77:467–501, 2018] for spatial discretization, we reformulate an extended linearized ODE system by the energy quadratization (EQ) approach. Second, we apply an s-stage algebraically stable RK method for temporal discretization. The resulting fully discrete DG schemes are linear and unconditionally energy stable. In addition, we introduce a prediction-correction procedure to improve both the accuracy and stability of the scheme. We illustrate the effectiveness of the proposed schemes by numerical tests with benchmark problems.

1. INTRODUCTION

In this paper, we are concerned with arbitrarily high order numerical approximations to a class of fourth order gradient flows,

$$u_t = -\mathcal{L}^2 u - \Phi'(u), \quad x \in \Omega, \quad t > 0, \quad (1.1)$$

where $\mathcal{L} = -(\Delta + a)$ is a second-order operator with a physical parameter a and Φ is a nonlinear function bounded from below. The model equation (1.1) governs the evolution of a scalar time-dependent unknown $u = u(x, t)$ in a convex domain $\Omega \subset \mathbb{R}^d$ and it describes important physical processes in nature. Typical examples of (1.1) include the Swift–Hohenberg equation [45] and the extended Fisher-Kolmogorov equation [10, 40]. There are other gradient flows such as the classical Allen–Cahn equation [1] and Cahn–Hilliard equation [4]. The common feature of gradient flow models is that the dynamics is driven by minimizing free energy.

We consider boundary conditions of form

$$(i) \ u \text{ is periodic;} \quad \text{or} \quad (ii) \ \partial_{\mathbf{n}} u = \partial_{\mathbf{n}} \Delta u = 0, \quad x \in \partial\Omega, \quad (1.2)$$

where \mathbf{n} stands for the unit outward normal to the boundary $\partial\Omega$. With such boundary conditions, equation (1.1) indeed features the energy dissipation property:

$$\frac{d}{dt} \mathcal{E}(u) = - \int_{\Omega} |u_t|^2 dx \leq 0, \quad (1.3)$$

2020 *Mathematics Subject Classification.* 65N12, 65N30, 35K35.

Key words and phrases. Gradient flows, RK method, EQ approach, DG methods, energy stability.

where the free energy

$$\mathcal{E}(u) = \int_{\Omega} \frac{1}{2} (\mathcal{L}u)^2 + \Phi(u) dx. \quad (1.4)$$

The model equation is nonlinear, its analytical solution is intractable. Hence designing accurate, efficient, and energy stable algorithms to solve it becomes essential. This energy dissipation law as a fundamental property of (1.1) has been explored in high order numerical approximations [15, 30, 32]. It was shown to be crucial to eliminate numerical results that are not physical. In this paper, we construct unconditionally energy stable and arbitrarily high order schemes to solve the above model problem, for which we use discontinuous Galerkin (DG) methods for spatial discretization, and high order Runge-Kutta (RK) methods for time discretization.

1.1. Related work. In the literature, there has been rapid development of different methods for simulating gradient flow models including (1.1), see e.g., [8, 9, 18, 26, 42, 12, 49, 50, 43, 53, 54, 46, 6]. They vary either in the spatial discretization or the time discretization, while the latter typically emphasizes preserving the energy dissipation property with no or mild time step restrictions. Let us briefly discuss existing works closely related to what we do here.

DG spatial discretization. It is known that for equations containing higher order spatial derivatives, DG discretization entails subtle difficulties in defining numerical fluxes. Several approaches have been developed to deal with the difficulties, including the local DG (LDG) methods [52, 11, 47], the mixed symmetric interior penalty (SIPG) methods [13, 14, 48, 16], and the ultra-weak DG [7]. To avoid certain drawbacks of these methods, a penalty free DG method was introduced in [29], where the symmetric structure of the model (1.1) is essentially used. This method still inherits the advantages of the usual DG methods, such as higher accuracy, flexibility in hp-adaption, capacity to handle domains with complex geometry [25, 22, 41, 44], its distinct feature lies in numerical fluxes without using any interior penalty. This is the spatial discretization we shall follow in this work.

EQ reformulation and time discretization. To keep the energy stability for gradient flow models, several time discretization techniques are available in the literature, including the so-called convex splitting [12, 49], and the stability approach [50, 43]. The former leads to nonlinear schemes, and the later often imposes restrictions on nonlinear terms in the model. The energy quadratization (EQ) approach introduced in [53, 54] turned to be rather general that it can be applied to a class of gradient flow models if the free energy is bounded below. Based on the idea of EQ, the scalar auxiliary variable (SAV) approach was introduced later in [46], where linear systems only with constant coefficients need to be solved. Several extensions of EQ and SAV have been further explored in [5, 23, 34, 51]. Earlier EQ based schemes are mostly up to 2nd order accurate in time, until recent works [20, 21], where the EQ formulation is combined with the Runge-Kutta methods to achieve high order in time schemes. Note that their schemes are fully nonlinear so that the solution existence and uniqueness are not guaranteed for large time steps. This issue is further addressed in [19] in which the obtained schemes are unconditionally energy stable and linear. We note that many existing EQ based schemes such as [53, 54, 19, 20, 21] use mainly finite-difference

or spectral methods for spatial discretization. New difficulties arise when coupling EQ with the DG discretization, as shown in [30, 31].

Integration of DG with EQ. Integration of EQ formulation with DG for solving (1.1) began with [30], where up to 2nd order (in time) IEQ-DG schemes are introduced. These schemes are shown to be unconditionally energy stable independent of the size of time steps, and easy to implement without resorting to any iteration method. A key point for the success in the scheme formulation is that the auxiliary energy variable is updated in point-wise manner, and then projected back into the DG space. This strategy of constructing the IEQ-DG schemes was further extended to solve the Cahn–Hilliard equation [31], where the spatial discretization is based on the DDG method [27, 28]. We note that a direct integration of the DG method with the SAV approach [46] will lead to linear systems involving dense coefficient matrices, hence rather expensive to solve. A special procedure was introduced in [32] as a rescue, so the resulting SAV-DG schemes become well positioned to solve (1.1). However, all these EQ/SAV based DG schemes are no more than second order in time.

Present investigation. The main purpose of this paper is to construct unconditionally energy stable DG schemes coupled with arbitrarily high order time discretization. We achieve this in two steps. First, taking advantage of the penalty free DG method introduced in [30], we reformulate an extended linearized ODE system by the energy quadratization (EQ) approach. Second, following [19], we apply an s -stage algebraically stable RK method for temporal discretization. The resulting fully discrete DG schemes are linear and unconditionally energy stable.

1.2. Our contribution.

- We construct the linear energy quadratized Runge-Kutta DG (LEQRK-DG) schemes to solve (1.1). In this construction we use a higher order interpolation in linearizing the extended EQ system, and a spatial projection for updating the auxiliary variable back into the DG space.
- We show that the LEQRK-DG schemes feature a discrete energy dissipation law for any time steps, hence these schemes are called unconditionally energy stable. We also propose LEQRK-DG-PC schemes following a prediction-correction procedure to improve both accuracy and stability of the LEQRK-DG schemes.
- We conduct experiments on benchmark examples to evaluate the performance of LEQRK-DG-PC method. First, we present numerical results to show the high order of spatial and temporal accuracy of the proposed schemes, and the energy dissipating properties of numerical solutions. Second, we conduct experiments on some two-dimensional pattern formation problems, all of which demonstrate the good performance of the LEQRK-DG-PC method.

1.3. Organization. In Section 2, we formulate a unified semi-discrete DG method for the gradient flow (1.1) subject to two different boundary conditions. In Section 3, we present LEQRK-DG schemes, and show the energy dissipation law. We also present the LEQRK-DG-PC method following a prediction-correction procedure. In Section 4, we verify the good performance of

LEQRK-DG-PC method using several benchmark numerical examples. Finally some concluding remarks are given in Section 5.

2. SPATIAL DG DISCRETIZATION

We derive mathematical formulation for our method. We begin with rewriting (1.1) as a mixed form

$$\begin{cases} u_t = -\mathcal{L}q - \Phi'(u), \\ q = \mathcal{L}u. \end{cases} \quad (2.1)$$

Such reformulation is not unique, the symmetric feature of (2.1) is essential for our DG method without the use of any interior penalty [29]. Let us recall some conventions of the DG discretization introduced in [29]. Let the domain Ω be a union of shape regular meshes $\mathcal{T}_h = \{K\}$, with the mesh size $h_K = \text{diam}\{K\}$ and $h = \max_K h_K$. We denote the set of the interior interfaces by Γ^0 , the set of all boundary faces by Γ^∂ , and the discontinuous Galerkin finite element space by

$$V_h = \{v \in L^2(\Omega) : v|_K \in P^k(K), \forall K \in \mathcal{T}_h\},$$

where $P^k(K)$ denotes the set of polynomials of degree no more than k on element K . If the normal vector on the element interface $e \in \partial K_1 \cap \partial K_2$ is oriented from K_1 to K_2 , then the average $\{\cdot\}$ and the jump $[\cdot]$ operator are defined by

$$\{v\} = \frac{1}{2}(v|_{\partial K_1} + v|_{\partial K_2}), \quad [v] = v|_{\partial K_2} - v|_{\partial K_1},$$

for any function $v \in V_h$, where $v|_{\partial K_i}$ ($i = 1, 2$) is the trace of v on e evaluated from element K_i .

Our DG discretization based on the mixed form (2.1) is to find $(u_h(\cdot, t), q_h(\cdot, t)) \in V_h \times V_h$ such that

$$(u_{ht}, \phi) = -G(q_h, \phi) - (\Phi'(u_h), \phi), \quad (2.2a)$$

$$(q_h, \psi) = G(u_h, \psi), \quad (2.2b)$$

for all $\phi, \psi \in V_h$. The precise form of $G(\cdot, \cdot)$ depending on the types of boundary conditions is given as follows:

$$\begin{aligned} G(w, v) &= \sum_{K \in \mathcal{T}_h} \int_K (\nabla w \cdot \nabla v - awv) dx + \sum_{e \in \Gamma^0} \int_e (\{\partial_\nu w\}[v] + [w]\{\partial_\nu v\}) ds \\ &\quad + \frac{\theta}{2} \int_{\Gamma^\partial} (\{\partial_\nu w\}[v] + [w]\{\partial_\nu v\}) ds, \end{aligned} \quad (2.3)$$

where $\theta = 1$ for (i) of (1.2) and $\theta = 0$ for (ii) of (1.2). Note that for periodic case (i) the left boundary and the right boundary are considered as same, for which we use the factor 1/2 to avoid recounting. The initial data for u_h is taken as the piecewise L^2 projection, denoted by $u_h(x, 0) = \Pi u_0(x)$.

The remarkable property of the above DG scheme is that the discrete energy of form

$$\mathcal{E}(u_h, q_h) := \frac{1}{2} \|q_h\|^2 + \int_{\Omega} \Phi(u_h) dx$$

admits a discrete dissipation law [29]:

$$\frac{d}{dt}\mathcal{E}(u_h, q_h) = - \int_{\Omega} |u_{ht}|^2 dx \leq 0. \quad (2.4)$$

3. TIME DISCRETIZATION

This section is devoted to arbitrarily higher order time discretization of the DG formulation (2.2).

First, we choose C_0 so that $\Phi(w) + C_0 > 0$, $\forall w \in \mathbb{R}$, and introduce

$$H(w) = \frac{\Phi'(w)}{\sqrt{\Phi(w) + C_0}}. \quad (3.1)$$

Then the IEQ reformulation of (2.2) requires to find $(u_h(\cdot, t), q_h(\cdot, t)) \in V_h \times V_h$ and U such that

$$(u_{ht}, \phi) = -G(\phi, q_h) - (H(u_h)U, \phi), \quad (3.2a)$$

$$(q_h, \psi) = G(u_h, \psi), \quad (3.2b)$$

$$U_t = \frac{1}{2}H(u_h)u_{ht}, \quad (3.2c)$$

for all $\phi, \psi \in V_h$. The initial data for the above scheme is chosen as

$$u_h(x, 0) = \Pi u_0(x), \quad U(x, 0) = \sqrt{\Phi(u_0(x)) + C_0},$$

where Π denotes the piecewise L^2 projection into V_h . Note that $U \notin V_h$.

There are two steps involved in the time discretization of (3.2). First, we utilize the numerical solutions of u_h for $t \leq t_n$ to obtain a high order approximation u_h^* , and replace the semi-discrete DG scheme (3.2) by

$$(u_{ht}, \phi) = -G(\phi, q_h) - (H(u_h^*)U, \phi), \quad (3.3a)$$

$$(q_h, \psi) = G(u_h, \psi), \quad (3.3b)$$

$$U_t = \frac{1}{2}H(u_h^*)u_{ht}. \quad (3.3c)$$

This linear scheme can be further solved in $t \in (t_n, t_{n+1}]$ by a high order ODE solver. We should point out that the above treatment does not destroy the energy dissipation property. Since for the modified energy functional

$$E(q_h, U) = \frac{1}{2}\|q_h\|^2 + \|U\|^2 = \mathcal{E}(u_h, q_h) + C_0|\Omega|$$

still satisfies

$$\frac{d}{dt}E(q_h, U) = - \int_{\Omega} |u_{ht}|^2 dx \leq 0.$$

Recall that for ODE of from $y_t = f(t, y)$, the general s-stage Runge–Kutta (RK) method has the form

$$y^{n+1} = y^n + \tau \sum_{i=1}^s b_i k_i,$$

where

$$k_i = f(t_n + c_i\tau, y^n + \tau \sum_{j=1}^s a_{ij}k_j), \quad i = 1, \dots, s.$$

Here for consistency the RK coefficients satisfy $c_i = \sum_{j=1}^s a_{ij}$ and $\sum_{i=1}^s b_i = 1$. For the convenience in applying the RK method to the semi-discrete DG schemes, we introduce the operator L_h by

$$(L_h v, \phi) = G(v, \phi) \quad \forall \phi \in V_h. \quad (3.4)$$

3.1. LEQRK-DG schemes. Applying a s-stage RK method to scheme (3.3), we obtain the following LEQRK-DG scheme.

Scheme 3.1. (s-stage LEQRK-DG scheme) For given u_h^n, U^n and $u_{ih}^{n,*} = u_h^*(x, t_n + c_i\tau)$, we find $(u_h^{n+1}, q_h^{n+1}, U_h^{n+1})$ by

$$u_h^{n+1} = u_h^n + \tau \sum_{i=1}^s b_i \xi_{ih}, \quad (3.5a)$$

$$q_h^{n+1} = L_h u_h^{n+1}, \quad (3.5b)$$

$$U^{n+1} = U^n + \tau \sum_{i=1}^s b_i l_i, \quad (3.5c)$$

$$U_h^{n+1} = \Pi U^{n+1}, \quad (3.5d)$$

where $\xi_{ih} \in V_h$ and l_i are determined by

$$(\xi_{ih}, \phi) = -G(\tilde{q}_{ih}, \phi) - \left(H(u_{ih}^{n,*}) \tilde{U}_i, \phi \right), \quad i = 1, 2, \dots, s \quad (3.6a)$$

$$(\tilde{q}_{ih}, \psi) = G(\tilde{u}_{ih}, \psi), \quad \forall \phi, \psi \in V_h, \quad (3.6b)$$

$$l_i = \frac{1}{2} H(u_{ih}^{n,*}) \xi_{ih}, \quad (3.6c)$$

and

$$\tilde{u}_{ih} = u_h^n + \tau \sum_{j=1}^s a_{ij} \xi_{jh}, \quad (3.7a)$$

$$\tilde{U}_i = U_h^n + \tau \sum_{j=1}^s a_{ij} l_j. \quad (3.7b)$$

Definition 3.1. (Algebraically stable RK method [3]) A RK method is algebraically stable if the RK coefficients satisfy stability conditions

$$b_i \geq 0, \quad i = 1, 2, \dots, s, \quad \text{and} \quad M \text{ is positive semi-definite}, \quad (3.8)$$

where M is a symmetric matrix with elements

$$M_{ij} = b_i a_{ij} + b_j a_{ji} - b_i b_j. \quad (3.9)$$

Next, we show that the algebraically stable LEQRK-DG scheme is unconditionally energy stable.

Theorem 3.1. The LEQRK-DG scheme with its RK coefficients satisfying the stability condition (3.8) is uniquely solvable for any $\tau > 0$ and unconditionally energy stable in the sense that

$$E_h^{n+1} \leq E_h^n - \tau \sum_{i=1}^s b_i \|\xi_{ih}\|^2, \quad (3.10)$$

where the energy

$$E_h^n := E(q_h^n, U_h^n) = \frac{1}{2} \|q_h^n\|^2 + \|U_h^n\|^2.$$

Proof. In order to prove (3.10), we use $\|U_h\| \leq \|U\|$ to obtain

$$E_h^{n+1} - E_h^n \leq \frac{1}{2} (\|q_h^{n+1}\|^2 - \|q_h^n\|^2) + (\|U_h^{n+1}\|^2 - \|U_h^n\|^2)$$

and estimate two terms on the right, respectively. First we have

$$\begin{aligned} \frac{1}{2} (\|q_h^{n+1}\|^2 - \|q_h^n\|^2) &= (q_h^{n+1} - q_h^n, q_h^{n+1}) - \frac{1}{2} \|q_h^{n+1} - q_h^n\|^2 \\ &= G(u_h^{n+1} - u_h^n, q_h^{n+1}) - \frac{1}{2} \|q_h^{n+1} - q_h^n\|^2 \\ &= \tau \sum_{i=1}^s b_i G(q_h^{n+1}, \xi_{ih}) - \frac{1}{2} \|q_h^{n+1} - q_h^n\|^2. \end{aligned}$$

Note that from (3.5ab), (3.6b) and (3.7a), we have

$$\begin{aligned} q_h^{n+1} &= L_h u_h^{n+1} = L_h u_h^n + \tau \sum_{j=1}^s b_j L_h \xi_{jh}, \\ \tilde{q}_{ih} &= L_h \tilde{u}_{ih} = L_h u_h^n + \tau \sum_{j=1}^s a_{ij} L_h \xi_{jh}. \end{aligned}$$

This gives

$$q_h^{n+1} = \tilde{q}_{ih} + \tau \left(\sum_{j=1}^s b_j L_h \xi_{jh} - \sum_{j=1}^s a_{ij} L_h \xi_{jh} \right),$$

which implies

$$G(q_h^{n+1}, \xi_{ih}) = G(\tilde{q}_{ih}, \xi_{ih}) + \tau \left(\sum_{j=1}^s b_j G(L_h \xi_{jh}, \xi_{ih}) - \sum_{j=1}^s a_{ij} G(L_h \xi_{jh}, \xi_{ih}) \right). \quad (3.11)$$

Setting $\phi = -\xi_{ih}$ in (3.6a), we have

$$\begin{aligned} -\|\xi_{ih}\|^2 &= G(\tilde{q}_{ih}, \xi_{ih}) + \left(H(u_{ih}^{n,*}) \tilde{U}_i, \xi_{ih} \right) \\ &= G(\tilde{q}_{ih}, \xi_{ih}) + 2(\tilde{U}_i, l_i), \end{aligned} \quad (3.12)$$

where we have used (3.6c) in the last step. Combining (3.12) with (3.11) gives

$$G(q_h^{n+1}, \xi_{ih}) = -\|\xi_{ih}\|^2 - 2(\tilde{U}_i, l_i) + \tau \left(\sum_{j=1}^s b_j G(L_h \xi_{jh}, \xi_{ih}) - \sum_{j=1}^s a_{ij} G(L_h \xi_{jh}, \xi_{ih}) \right).$$

Further, using (3.5ab), we obtain

$$\begin{aligned} \frac{1}{2} \|q_h^{n+1} - q_h^n\|^2 &= \frac{1}{2} (L_h u_h^{n+1} - L_h u_h^n, L_h u_h^{n+1} - L_h u_h^n) \\ &= \frac{1}{2} \tau^2 \sum_{i,j=1}^s b_i b_j (L_h \xi_{ih}, L_h \xi_{jh}) \\ &= \frac{1}{2} \tau^2 \sum_{i,j=1}^s b_i b_j G(\xi_{ih}, L_h \xi_{jh}). \end{aligned}$$

For the second term we use (3.5c) to obtain

$$\begin{aligned} \|U^{n+1}\|^2 - \|U_h^n\|^2 &= 2(U^{n+1}, U^{n+1} - U_h^n) - \|U^{n+1} - U_h^n\|^2 \\ &= 2(U^{n+1}, \tau \sum_{i=1}^s b_i l_i) - (U^{n+1} - U_h^n, U^{n+1} - U_h^n) \\ &= 2\tau \sum_{i=1}^s b_i (U^{n+1}, l_i) - \tau^2 \sum_{i,j=1}^s b_i b_j (l_i, l_j). \end{aligned}$$

Putting together all these estimates,

$$\begin{aligned} E_h^{n+1} - E_h^n &\leq -\frac{1}{2} \tau^2 \sum_{i,j=1}^s b_i b_j G(\xi_{ih}, L_h \xi_{jh}) - \tau^2 \sum_{i,j=1}^s b_i b_j (l_i, l_j) \\ &\quad + \tau \sum_{i=1}^s b_i G(q_h^{n+1}, \xi_{ih}) + 2\tau \sum_{i=1}^s b_i (U^{n+1}, l_i) \\ &\leq -\tau^2 \sum_{i,j=1}^s b_i b_j (l_i, l_j) - \tau \sum_{i=1}^s b_i \|\xi_{ih}\|^2 + 2\tau \sum_{i=1}^s b_i (U^{n+1} - \tilde{U}_i, l_i) \\ &\quad + \tau^2 \left(\frac{1}{2} \sum_{i,j=1}^s b_i b_j G(L_h \xi_{jh}, \xi_{ih}) - \sum_{i,j=1}^s b_i a_{ij} G(L_h \xi_{jh}, \xi_{ih}) \right). \end{aligned}$$

Subtracting (3.7b) from (3.5c) gives

$$U^{n+1} - \tilde{U}_i = \tau \sum_{j=1}^s b_j l_j - \tau \sum_{j=1}^s a_{ij} l_j.$$

Hence

$$2\tau \sum_{i=1}^s b_i (U^{n+1} - \tilde{U}_i, l_i) = 2\tau^2 \left(\sum_{i,j=1}^s b_i b_j (l_i, l_j) - \sum_{i,j=1}^s b_i a_{ij} (l_i, l_j) \right).$$

Combining the results above, we have

$$\begin{aligned} E_h^{n+1} - E_h^n &\leq -\tau \sum_{i=1}^s b_i \|\xi_{ih}\|^2 - \frac{\tau^2}{2} \sum_{i,j=1}^s M_{ij}(L_h \xi_{ih}, L_h \xi_{jh}) - \tau^2 \sum_{i,j=1}^s M_{ij}(l_i, l_j) \\ &\leq -\tau \sum_{i=1}^s b_i \|\xi_{ih}\|^2, \end{aligned}$$

where we have used (3.8).

It is left to prove the unique solvability of the fully discrete scheme, for which it suffices to prove the linear scheme admits only a zero solution if $u_h^n = 0$ and $U^n = 0$. In fact from $E_h^n = 0$, the energy dissipation inequality above tells that

$$\frac{1}{2}\|q_h^{n+1}\|^2 + \|U^{n+1}\|^2 + \tau \sum_{i=1}^s b_i \|\xi_{ih}\|^2 + \frac{\tau^2}{2} \sum_{i,j=1}^s M_{ij}(L_h \xi_{ih}, L_h \xi_{jh}) + \tau^2 \sum_{i,j=1}^s M_{ij}(l_i, l_j) \leq 0.$$

This therefore ensures that

$$q_h^{n+1} = 0, U^{n+1} = 0, \quad i = 1, \dots, s,$$

and $b_i \xi_{ih} = 0$ for $i = 1 \dots s$, so $u_h^{n+1} = \tau \sum_{i=1}^s b_i \xi_{ih} = 0$. \square

Remark 3.1. To ensure the energy stability it suffices to take $C_0 > -\inf \Phi(u)$. However, a larger C_0 can help to reduce the spatial projection error when associated with the DG discretization. For example, let ΠU_0 be the piecewise L^2 projection of U_0 in V_h based on P^1 polynomials, then the projection error is known as

$$\|U_0 - \Pi U_0\| = Ch|U_0|_{H^1(\Omega)}, \quad (3.13)$$

where C independent of h and U_0 . Note that

$$|U_0|_{H^1(\Omega)}^2 = \sum_{K \in \Omega} \int_K \left(\frac{\Phi'(u_0)}{\sqrt{\Phi(u_0) + C_0}} \right)^2 |\nabla u_0|^2 dx,$$

from which we see that a larger C_0 will reduce the total error.

Remark 3.2. System (3.6) may be put as a closed linear system as

$$\begin{aligned} (\xi_{ih}, \phi) + \frac{\tau}{2} \sum_{j=1}^s a_{ij} (H(u_{ih}^{n,*})^2 \xi_{jh}, \phi) + G(\tilde{q}_{ih}, \phi) &= - (H(u_{ih}^{n,*}) U_h^n, \phi), \\ \tau \sum_{j=1}^s a_{ij} G(\xi_{jh}, \psi) - (\tilde{q}_{ih}, \psi) &= - G(u_h^n, \psi), \end{aligned}$$

where the first equation is obtained by plugging (3.7b) as well as (3.6c) into (3.6a), and the second equation is obtained by plugging (3.7a) into (3.6b).

Remark 3.3. A variety of algebraically stable RK methods have been introduced in the literature, see, e.g., [3]. Here we present three methods in the form of the Butcher tableau. Qin and Zhang's two-stage, second order diagonally implicit RK method [39]

$$\begin{array}{c|c} \mathbf{c} & A \\ \hline & \mathbf{b}^\mathbf{T} \end{array} = \begin{array}{c|cc} \frac{1}{4} & \frac{1}{4} & 0 \\ \frac{3}{4} & \frac{1}{2} & \frac{1}{4} \\ \hline & \frac{1}{2} & \frac{1}{2} \end{array}, \quad M = \begin{bmatrix} 0 & 0 \\ 0 & 0 \end{bmatrix}, \quad (3.14)$$

Crouzeix's two-stage, third order diagonally implicit RK method [36],

$$\begin{array}{c|c} \mathbf{c} & A \\ \hline & \mathbf{b}^\mathbf{T} \end{array} = \begin{array}{c|cc} \frac{1}{2} + \frac{\sqrt{3}}{6} & \frac{1}{2} + \frac{\sqrt{3}}{6} & 0 \\ \frac{1}{2} - \frac{\sqrt{3}}{6} & -\frac{\sqrt{3}}{3} & \frac{1}{2} + \frac{\sqrt{3}}{6} \\ \hline & \frac{1}{2} & \frac{1}{2} \end{array}, \quad M = \left(\frac{1}{4} + \frac{\sqrt{3}}{6} \right) \begin{bmatrix} 1 & -1 \\ -1 & 1 \end{bmatrix}, \quad (3.15)$$

and the two-stage, fourth order Gauss-Legendre method [24]:

$$\left. \begin{array}{c|c} \mathbf{c} & A \\ \hline & \mathbf{b}^T \end{array} \right| = \left. \begin{array}{cc|cc} \frac{1}{2} - \frac{\sqrt{3}}{6} & & \frac{1}{4} & \frac{1}{4} - \frac{\sqrt{3}}{6} \\ \frac{1}{2} + \frac{\sqrt{3}}{6} & & \frac{1}{4} + \frac{\sqrt{3}}{6} & \frac{1}{4} \\ \hline & & \frac{1}{2} & \frac{1}{2} \end{array} \right|, \quad M = \begin{bmatrix} 0 & 0 \\ 0 & 0 \end{bmatrix}. \quad (3.16)$$

These RK methods will be adopted in our numerical experiments.

Remark 3.4. For RK methods with Butcher tableau

$$\left. \begin{array}{c|c} \mathbf{c} & A \\ \hline & \mathbf{b}^T \end{array} \right| = \left. \begin{array}{c|c} 1 & 1 \\ \hline & 1 \end{array} \right|, \quad \left. \begin{array}{c|c} \mathbf{c} & A \\ \hline & \mathbf{b}^T \end{array} \right| = \left. \begin{array}{c|c} \frac{1}{2} & \frac{1}{2} \\ \hline & 1 \end{array} \right|,$$

Scheme 3.1 reduces to the first order, second order IEQ-DG schemes in [30], respectively.

To complete Scheme 3.1, we discuss how to prepare u_h^* , hence $u_{ih}^{n,*}$. For $n = 0$, we take

$$u_h^0 = \Pi u_0, \quad u_{ih}^{0,*} = u_h^0.$$

For $n \geq 1$, we construct a Lagrangian interpolating polynomial u_h^* based on $s + 2$ points:

$$(t_{n-1}, u_h^{n-1}), (t_{n-1} + c_i\tau, \tilde{u}_{ih}), (t_n, u_h^n),$$

and set

$$u_{ih}^{n,*} = u_h^*(x, t_n + c_i\tau).$$

However, two drawbacks might show up with this simple interpolation: (i) when s is large, interpolating polynomials may be highly oscillatory, leading to instability or inaccuracy of the extrapolation from $[t_{n-1}, t_n]$ to $(t_n, t_{n+1}]$; (ii) the order of accuracy of the interpolation can be lower than the order of the RK method, putting another restriction on the overall accuracy of the resulting scheme. The Gauss-Legendre method in (3.16) is a such example.

3.2. LEQRK-DG-PC method. In order to improve the stability as well as the accuracy of Scheme 3.1 we propose a prediction-correction method, following the strategy in [17, 19]. To do so, we also need the Lagrangian interpolation polynomial $U_h^*(x, t)$ based on the interpolation points

$$(t_{n-1}, U_h^{n-1}), (t_{n-1} + c_i\tau, \tilde{U}_{ih}) \text{ and } (t_n, U_h^n), i = 1, 2, \dots, s.$$

Here, $\tilde{U}_{ih} = \Pi \tilde{U}_i$ is the piecewise L^2 projection of \tilde{U}_i in (3.7b) from $(t_{n-1}, t_n]$.

Scheme 3.2. (s -stage LEQRK-DG-PC scheme) For given $u_h^n, U_h^n, u_h^*(x, t_n + c_i\tau)$ and $U_h^*(x, t_n + c_i\tau)$, $i = 1, 2, \dots, s$, a s -stage LEQRK-DG-PC scheme is given as follows.

Prediction: Set $\tilde{u}_{ih}^0 = u_h^*(x, t_n + c_i\tau)$, $\tilde{U}_{ih}^0 = U_h^*(x, t_n + c_i\tau)$, we iteratively solve

$$(\xi_{ih}^{m+1}, \phi) = -G(\tilde{q}_{ih}^{m+1}, \phi) - \left(H(\tilde{u}_{ih}^m) \tilde{U}_{ih}^m, \phi \right), \quad (3.17a)$$

$$(\tilde{q}_{ih}^{m+1}, \psi) = G(\tilde{u}_{ih}^{m+1}, \psi), \quad \forall \phi, \psi \in V_h, \quad (3.17b)$$

and

$$\tilde{u}_{ih}^{m+1} = u_h^n + \tau \sum_{j=1}^s a_{ij} \xi_{jh}^{m+1}, \quad (3.18a)$$

$$l_i^{m+1} = \frac{1}{2} H(\tilde{u}_{ih}^{m+1}) \xi_{ih}^{m+1}, \quad (3.18b)$$

$$\tilde{U}_i^{m+1} = U_h^n + \tau \sum_{j=1}^s a_{ij} l_j^{m+1}, \quad (3.18c)$$

$$\tilde{U}_{ih}^{m+1} = \Pi \tilde{U}_i^{m+1}. \quad (3.18d)$$

If $\max_i \|\tilde{u}_{ih}^{m+1} - \tilde{u}_{ih}^m\|_\infty < Tol$, we stop the iteration and set $u_{ih}^{n,*} = \tilde{u}_{ih}^{m+1}$; otherwise, we set $u_{ih}^{n,*} = \tilde{u}_{ih}^L$, where $L > 0$ is a priori given integer.

Correction: With the predicted $u_{ih}^{n,*}$, we apply Scheme 3.1 to update the numerical solutions, and also set

$$\tilde{U}_{ih} = \Pi \tilde{U}_i$$

for the update in the next time step.

Remark 3.5. If $L = 0$, the LEQRK-DG-PC scheme reduces to Scheme 3.1.

4. NUMERICAL RESULTS

In this section, we numerically test the orders of convergence of the proposed LEQRK-DG-PC schemes. Further, we apply the schemes to the 2D Swift-Hohenberg equation in order to recover some known patterns, while we also verify the unconditional energy stability at the same time.

The experimental orders of convergence (EOC) at $T = n\tau$ in terms of h and τ are determined respectively by

$$\text{EOC} = \log_2 \left(\frac{e_h^n}{e_{h/2}^n} \right), \quad \text{EOC} = \log_2 \left(\frac{e_h^n}{e_h^{2n}} \right),$$

where e_h^n represents the error between the numerical solution $u_h^n(x, y)$ and the exact solution $u(x, y, t^n)$, and e_h^{2n} corresponds to the numerical solution with $\tau/2$ as the time step.

The Swift-Hohenberg equation is a special case of model equation (1.1) with $a = 1$ and

$$\Phi(u) = -\frac{\epsilon}{2}u^2 - \frac{g}{3}u^3 + \frac{u^4}{4}, \quad (4.1)$$

that is,

$$u_t = -\Delta^2 u - 2\Delta u + (\epsilon - 1)u + gu^2 - u^3. \quad (4.2)$$

Here physical parameters are $g \geq 0$ and $\epsilon \in \mathbb{R}$, which together with the size of the domain play an important role in pattern selection; see, e.g., [2, 37, 35]. In our numerical tests, we focus on (4.1) with $g \geq 0$ and $\epsilon > 0$. This function has double wells with two local minimal values at $u_\pm = \frac{g \pm \sqrt{g^2 + 4\epsilon}}{2}$ such that $\Phi'(u_\pm) = 0$, and

$$\Phi(u) \geq \min\{\Phi(u_\pm)\} = \min_{v=u_\pm} \left(-\frac{1}{12} (gv(g^2 + 4\epsilon) + \epsilon(g^2 + 3\epsilon)) \right) = -b,$$

so it suffices to choose the method parameter $C_0 \geq b$. In all numerical examples $b < 1$, together with the discussion in Remark 3.1, we will take $C_0 = 10^3$ for all examples.

Example 4.1. (Spatial accuracy test) Consider the Swift-Hohenberg equation (4.2) with an added source of form

$$f(x, y, t) = -\varepsilon v - gv^2 + v^3, \quad v := e^{-t/4} \sin(x/2) \sin(y/2),$$

subject to initial data

$$u_0(x, y) = \sin(x/2) \sin(y/2). \quad (4.3)$$

This problem has an explicit solution

$$u(x, y, t) = e^{-t/4} \sin(x/2) \sin(y/2). \quad (4.4)$$

To be specific, we take $\varepsilon = 0.025$, $g = 0$, and domain $\Omega = [-2\pi, 2\pi]^2$ with periodic boundary conditions. We shall test the LEQRK-DG-PC scheme based on the RK method with Butcher tableau (3.16) and P^k polynomials. Note that due to the source term, we need to add

$$(f(\cdot, t^n + b_i\tau), \phi),$$

to the right hand side of both (3.6a) and (3.17a). In prediction step, we take $L = 10$ and tolerance $Tol = 10^{-10}$. This example is used to test the spatial accuracy, using polynomials of degree k with $k = 1, 2, 3$ on 2D rectangular meshes. Both errors and orders of convergence at $T = 0.01$ are reported in Table 1. These results confirm the $(k + 1)$ th orders of accuracy in L^2, L^∞ norms.

TABLE 1. L^2, L^∞ errors and EOC at $T = 0.01$ with mesh $N \times N$.

k	τ		N=8	N=16		N=32		N=64	
			error	error	order	error	order	error	order
1	1e-3	$\ u - u_h\ _{L^2}$	3.73985e-01	9.73764e-02	1.94	2.39651e-02	2.02	5.95959e-03	2.01
		$\ u - u_h\ _{L^\infty}$	1.38441e-01	3.83905e-02	1.85	9.61382e-03	2.00	2.40153e-03	2.00
2	1e-4	$\ u - u_h\ _{L^2}$	7.10034e-02	1.50739e-02	2.24	2.02727e-03	2.89	2.58614e-04	2.97
		$\ u - u_h\ _{L^\infty}$	2.41033e-02	3.22536e-03	2.90	4.40302e-04	2.87	5.63426e-05	2.97
3	2e-5	$\ u - u_h\ _{L^2}$	1.20130e-02	1.13186e-03	3.41	7.72408e-05	3.87	4.94306e-06	3.97
		$\ u - u_h\ _{L^\infty}$	3.85682e-03	3.68735e-04	3.39	2.43500e-05	3.92	1.53904e-06	3.98

Example 4.2. (Temporal accuracy test) Consider the Swift-Hohenberg equation (4.2) with an added source of form

$$f(x, y, t) = -\varepsilon v - gv^2 + v^3, \quad v := e^{-49t/64} \sin(x/4) \sin(y/4),$$

subject to initial data

$$u_0(x, y) = \sin(x/4) \sin(y/4). \quad (4.5)$$

Its exact solution is given by

$$u(x, y, t) = e^{-49t/64} \sin(x/4) \sin(y/4).$$

We want to test the temporal accuracy of the LEQRK-DG-PC method, for which we take $\varepsilon = 0.025$, $g = 0$, and domain $\Omega = [-4\pi, 4\pi]^2$ with periodic boundary conditions. We apply the two-stage LEQRK-DG-PC schemes based on second, third and fourth order RK methods with Butcher tableau (3.14)-(3.16) and P^3 polynomials. Similar to Example 4.1, we also need to add

$$(f(\cdot, t^n + b_i\tau), \phi),$$

to the right hand side of both (3.6a) and (3.17a). We take time steps $\tau = 2^{-m}$ for $2 \leq m \leq 5$ and mesh size 64×64 . In the prediction step, we choose the tolerance $Tol = 10^{-10}$ and the value of L depends on the specific RK methods. The L^2, L^∞ errors and orders of convergence at $T = 1.5$ are shown in Table 2, and these results confirm that the schemes as tested can achieve the optimal orders of convergence in time.

TABLE 2. L^2, L^∞ errors and EOC at $T = 1.5$ with time step τ .

RK	L		$\tau = 2^{-2}$	$\tau = 2^{-3}$		$\tau = 2^{-4}$		$\tau = 2^{-5}$	
			error	error	order	error	order	error	order
(3.14)	0	$\ u - u_h\ _{L^2}$	5.84575e-02	1.29975e-02	2.17	3.21365e-03	2.02	8.05270e-04	2.00
		$\ u - u_h\ _{L^\infty}$	5.51717e-03	1.13568e-03	2.28	2.80093e-04	2.02	7.04859e-05	1.99
(3.15)	2	$\ u - u_h\ _{L^2}$	6.49591e-03	7.15397e-04	3.18	8.88739e-05	3.01	9.69107e-06	3.20
		$\ u - u_h\ _{L^\infty}$	7.59053e-04	1.09547e-04	2.79	1.37766e-05	2.99	1.46945e-06	3.23
(3.16)	2	$\ u - u_h\ _{L^2}$	2.10020e-03	1.38306e-04	3.92	7.30941e-06	4.24	--	--
		$\ u - u_h\ _{L^\infty}$	3.43273e-04	2.20772e-05	3.96	1.42833e-06	3.95	--	--

Example 4.3. (Rolls and Hexagons) In this example, we simulate the formation and evolution of patterns of the the Swift-Hohenberg equation (4.2), which arises in the Rayleigh-Bénard convection. Following [38, 30], we run the simulation from $t = 0$ to $t = 198$ on a rectangular domain $\Omega = [0, 100]^2$, subject to random initial data and periodic boundary conditions. Model parameters ε , g will be specified below for different cases.

We apply the LEQRK-DG-PC scheme based on the fourth order RK method with Butcher tableau (3.16) and P^2 polynomials using mesh 128×128 . We take time step $\tau = 0.1$, which is much larger than that used in [38, 30]. In the following two test cases, we output $E(q_h^n, U_h^n) - C_0|\Omega|$ instead of $E(q_h^n, U_h^n)$ to better observe the evolution of the original free energy $\mathcal{E}(u)$.

Test case 1. (Rolls) For parameters $\varepsilon = 0.3$, $g = 0$, we observe the periodic rolls for different times as shown in Figure 1. We see that the pattern evolves approaching the steady-state after $t > 60$, as also evidenced by the energy evolution plot in Figure 3a.

Test case 2. (Hexagons) The numerical simulations with the parameters $\varepsilon = 0.1$, $g = 1.0$ reveal vividly the formation and evolution of the hexagonal pattern as shown in Figure 2. The pattern at $t = 1.2$ is similar to that of rolls as shown in Figure 1. Similar to the pattern obtained by the IEQ-DG scheme in [30], we also observe that at a certain point before $t = 40$, lines break up giving way to single droplets that take hexagonal symmetry. The steady state is approaching after $t > 100$.

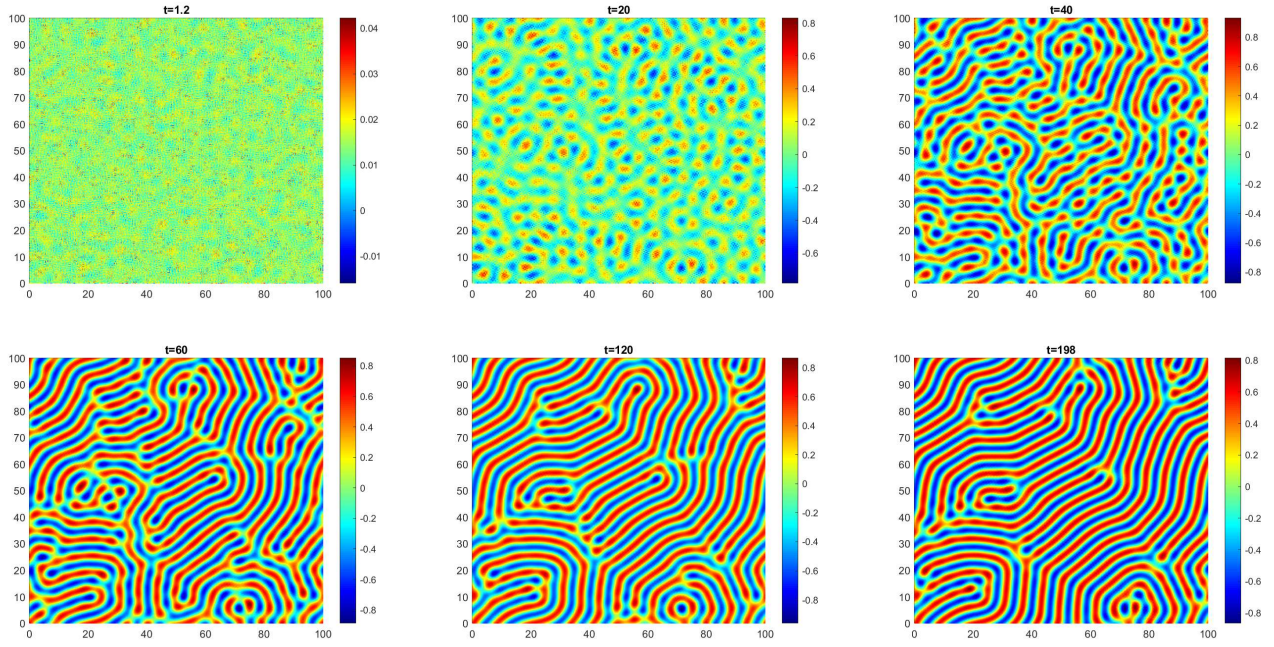


FIGURE 1. Evolution of periodic rolls.

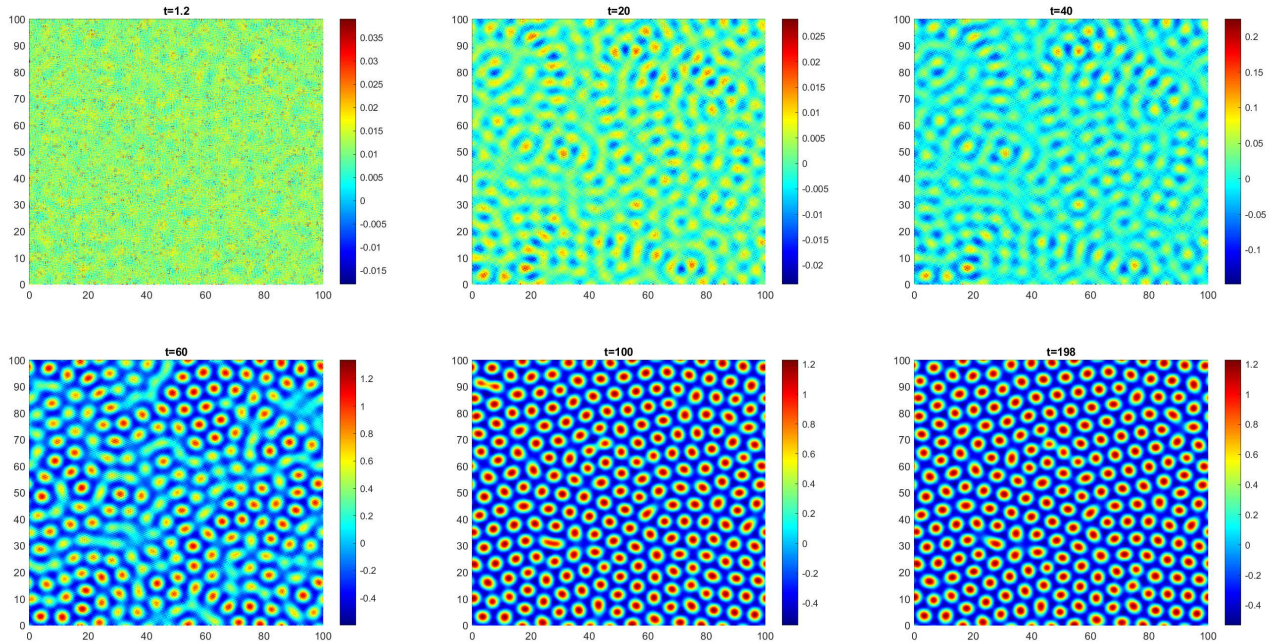


FIGURE 2. Evolution of hexagonal patterns.

The evolution of the patterns for both cases is shown to satisfy the energy dissipation law in Figure 3. With the same parameters ε , g as in [30], the LEQRK-DG-PC scheme can generate quite similar formation and evolution of both roll and hexagonal patterns even with a larger time step.

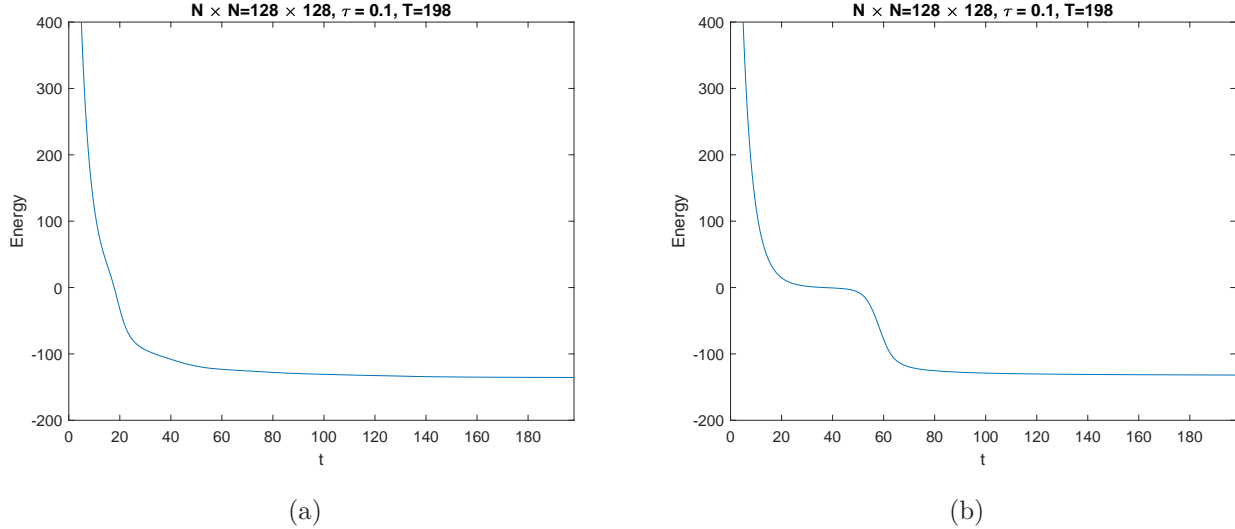


FIGURE 3. Energy evolution. (a) Rolls. (b) Hexagons.

5. CONCLUDING REMARKS

In this paper, we present a new class of arbitrarily high order, fully discrete DG schemes. These schemes have several advantageous properties: (1) the schemes are all linear such that they are easy to implement and computationally efficient; (2) the schemes are uniquely solvable and unconditionally energy stable, these ensure that large time steps can be used in some long time simulations; (3) the schemes can reach arbitrarily high order of accuracy in both space and time, so that desired accuracy of solutions can be guaranteed with flexible meshes and time steps; (4) the schemes do not depend on the specific form of the DG operator explicitly such that it can be applied to a larger class of DG schemes as long as they satisfy a semi-discrete energy dissipation law. The proofs for energy stability are given. Several numerical examples are presented to assess the scheme performance in terms of accuracy and energy stability. The numerical results on two dimensional pattern formation problems indicate that the method is able to deliver expected patterns of high accuracy with a larger time step on coarse meshes.

ACKNOWLEDGMENTS

This research was supported by the National Science Foundation under Grant DMS1812666.

REFERENCES

- [1] S. M. Allen and J. W. Cahn. A microscopic theory for antiphase boundary motion and its application to antiphase domain coarsening. *Acta. Metall.*, 27:1085–1095, 1979.
- [2] G. J. B. van den Berg, L. A. Peletier and W. C. Troy. Global branches of multi-bump periodic solutions of the Swift–Hohenberg equation. *Arch. Rational Mech. Anal.*, 158:91–153, 2001.
- [3] K. Burrage and J. C. Butcher. Stability criteria for implicit Runge–Kutta methods. *SIAM J. Numer. Anal.*, 16(1):46–57, 1979.

- [4] J. W. Cahn and J. E. Hilliard. Free energy of a nonuniform system. I. interfacial free energy. *J. Chem. Phys.*, 28:258–267, 1958.
- [5] L. Chen, J. Zhao, and X. Yang. Regularized linear schemes for the molecular beam epitaxy model with slope selection. *Applied Numerical Mathematics*, 128:138–156, 2018.
- [6] W. Chen, C. Wang, X. Wang, S. M. Wise. Positivity-preserving, energy stable numerical schemes for the Cahn-Hilliard equation with logarithmic potential. *J. Comput. Phys.: X*, 3:100031, 2019.
- [7] Y. Cheng and C.-W. Shu. A discontinuous Galerkin finite element method for time dependent partial differential equations with higher order derivatives. *Math. Comp.*, 77:699–730, 2008.
- [8] C. I. Christov and J. Pontes. Numerical scheme for Swift–Hohenberg equation with strict implementation of Lyapunov functional. *Math. Comput. Modelling*, 35:87–99, 2002.
- [9] C. I. Christov, J. Pontes, D. Walgraef and M. G. Velarde. Implicit time splitting for fourth-order parabolic equations. *Comput. Methods Appl. Mech. Engrg.*, 148:209–224, 1997.
- [10] G. Dee and W. Saarloos. Bistable systems with propagating fronts leading to pattern formation. *Phys. Rev. Lett.*, 60:2641–2644, 1988.
- [11] B. Dong and C.-W. Shu. Analysis of a local discontinuous Galerkin method for linear time-dependent fourth-order problems. *SIAM J. Numer. Anal.*, 47(5):3240–3268, 2009.
- [12] D. J. Eyre. Unconditionally gradient stable time marching the Cahn-Hilliard equation. In Computational and mathematical models of microstructural evolution (San Francisco, CA, 1998), volume 529 of Mater. Res. Soc. Sympos. Proc., pages 39–46. MRS, 1998.
- [13] X. Feng and O. A. Karakashian. Fully discrete dynamic mesh discontinuous Galerkin methods for the Cahn-Hilliard equation of phase transition. *Math. Comp.*, 76:1093–1117, 2007.
- [14] X. Feng, Y. Li and Y. Xing. Analysis of mixed interior penalty discontinuous Galerkin methods for the Cahn-Hilliard equation and the Hele-Shaw flow. *SIAM J. Numer. Anal.*, 54(2):825–847, 2016.
- [15] P. C. Fife and M. Kowalczyk. A class of pattern-forming models. *J. Nonlinear Sci.*, 9:641–669, 1999.
- [16] A. S.-Filibelioglu, B. Karasözen and M. Uzunca. Energy stable interior penalty discontinuous Galerkin finite element method for Cahn-Hilliard equation. *Int. J. Nonlinear Sci. Numer. Simul.*, 18(5):303–314, 2017.
- [17] K. Glasner and S. Orizaga. Improving the accuracy of convexity splitting methods for gradient flow equations. *J. Comput. Phys.*, 315:52–64, 2016.
- [18] H. Gomez and X. Nogueira. A new space-time discretization for the Swift–Hohenberg equation that strictly respects the Lyapunov functional. *Commun. Nonlinear Sci. Numer. Simulat.*, 17(12):4930–4946, 2012.
- [19] Y. Gong, J. Zhao and Q. Wang. Arbitrarily high-order linear energy stable schemes for gradient flow models. *J. Comput. Phys.*, 419:109610, 2020.
- [20] Y. Gong, J. Zhao and Q. Wang. Arbitrarily high-order unconditionally energy stable SAV schemes for gradient flow models. *Computer Physics Communications*, 249:107033, 2020.
- [21] Y. Gong, J. Zhao and Q. Wang. Arbitrarily high-order unconditionally energy stable schemes for thermodynamically consistent gradient flow models. *SIAM Journal on Scientific Computing*, 42(1):B135–B156, 2020.
- [22] J. S. Hesthaven and T. Warburton. Nodal Discontinuous Galerkin Methods: Algorithms, Analysis, and Applications. Springer, New York, 2007.
- [23] D. Hou, M. Azaiez, and C. Xu. A variant of scalar auxiliary variable approaches for gradient flows. *J. Comput. Phys.*, 395:307–332, 2019.
- [24] A. Iserles. A First Course in the Numerical Analysis of Differential Equations. *Cambridge University Press*, 1996.
- [25] R. M. Kirby, T. C. Warburton, I. Lomtev and G.E. Karniadakis. A discontinuous Galerkin spectral/*hp* method on hybrid grids. *Applied Numerical Mathematics*, 33:393–405, 2000.
- [26] H. G. Lee. A semi-analytical Fourier spectral method for the Swift–Hohenberg equation. *Computers & Mathematics with Applications (CMA)*, 74(8):1885–1896, 2017.

- [27] H. Liu and J. Yan. The Direct Discontinuous Galerkin (DDG) method for diffusion problems. *SIAM Journal on Numerical Analysis*, 47(1):675–698, 2009.
- [28] H. Liu and J. Yan. The Direct Discontinuous Galerkin (DDG) method for diffusion with interface corrections. *Commun. Comput. Phys.*, 8(3):541–564, 2010.
- [29] H. Liu and P. Yin. A mixed discontinuous Galerkin method without interior penalty for time-dependent fourth order problems. *J. Sci. Comput.*, 77:467–501, 2018.
- [30] H. Liu and P. Yin. Unconditionally energy stable DG schemes for the Swift-Hohenberg equation. *J. Sci. Comput.*, 81:789–819, 2019.
- [31] H. Liu and P. Yin. Unconditionally energy stable DG schemes for the Cahn-Hilliard equation. *arXiv preprint*, arXiv:1912.10197, 2019.
- [32] H. Liu and P. Yin. On the SAV-DG method for a class of fourth order gradient flows. *arXiv preprint*, arXiv:2008.11877, 2020.
- [33] Y. Liu, Q. Tao and C.-W. Shu. Analysis of optimal superconvergence of an ultra-weak local discontinuous Galerkin method for a time dependent fourth-order equation. *ESAIM: Mathematical Modelling and Numerical Analysis*, 54:1797–1820, 2020.
- [34] Z. Liu and X. Li. Efficient modified techniques of invariant energy quadratization approach for gradient flows. *Applied Math. Letters*, 98:206–214, 2019.
- [35] D. Morgan, J. H. P. Dawes. The Swift-Hohenberg equation with a nonlocal nonlinearity. *Physica D: Nonlinear Phenomena*, 270(1):60–80, 2014.
- [36] S.P. Nørsett. Semi-explicit Runge-kutta Methods. *Department of Mathematics, University of Trondheim*, 1974.
- [37] L. A. Peletier and V. Rottschäfer. Pattern selection of solutions of the Swift–Hohenberg equation. *Physica D: Nonlinear Phenomena*, 194(1):95–126, 2004.
- [38] S. S. Pérez-Moreno, S. R. Chavarría and G. R. Chavarría. Numerical solution of the Swift–Hohenberg equation. In: *J. Klapp, A. Medina (eds). Experimental and Computational Fluid Mechanics. Environmental Science and Engineering. Springer, Cham.*, 409–416, 2014.
- [39] M. Z. Qin and M. Q. Zhang. Symplectic Runge-Kutta algorithms for Hamiltonian systems. *J. Comput. Math. (Suppl.)*, 205-215, 1992.
- [40] L. A. Peletier and W. C. Troy. Spatial patterns described by the extended Fisher-Kolmogorov (EFK) equation: kinks. *Differ. Integral Equ.*, 8:1279–1304, 1995.
- [41] B. Rivière. *Discontinuous Galerkin Methods for Solving Elliptic and Parabolic Equations*. Society for Industrial and Applied Mathematics, 2008.
- [42] A. F. Sarmiento, L. F. R. Espath, P. Vignal, L. Dalcin, M. Parsani and V. M. Calo. An energy-stable generalized- α method for the Swift–Hohenberg equation. *J. Comput. Appl. Math.*, 344:836–851, 2018.
- [43] J. Shen and X. Yang. Numerical approximations of Allen-Cahn and Cahn-Hilliard equations. *Discrete Contin. Dyn. Syst. A*, 28:1669–1691, 2010.
- [44] C.-W. Shu. Discontinuous Galerkin methods: general approach and stability. In *Numerical solutions of partial differential equations*, Adv. Courses Math. CRM Barcelona, pages 149–201. Birkhäuser, Basel, 2009.
- [45] J. Swift and P. C. Hohenberg. Hydrodynamic fluctuations at the convective instability. *Physical Review A*, 15:319–328, 1977.
- [46] J. Shen, J. Xu and X. Yang. The scalar auxiliary variable (SAV) approach for gradient flows. *J. Comput. Phys.*, 353:407–416, 2018.
- [47] H. Wang, Q. Zhang and C.-W. Shu. Stability analysis and error estimates of local discontinuous Galerkin methods with implicit-explicit time-marching for the time-dependent fourth order PDEs. *ESAIM: M2AN*, 51:1931–1955, 2017.
- [48] G. N. Wells. E. Kuhl and K. Garikipati. A discontinuous Galerkin method for the Cahn-Hilliard equation. *J. Comput. Phys.*, 218:860–877, 2006.

- [49] X. Wu, G. J. v. Zwieten and K. G. v. d. Zee. Stabilized second-order convex splitting schemes for Cahn-Hilliard models with application to diffuse-interface tumor-growth models. *Int. J. Numer. Meth. Biomed. Engng.*, 30:180–203, 2014.
- [50] C. Xu and T. Tang. Stability analysis of large time-stepping methods for epitaxial growth models. *SIAM. J. Num. Anal.*, 44:1759–1779, 2006.
- [51] Z. Xu, X. Yang, H. Zhang, and Z. Xie. Efficient and linear schemes for anisotropic Cahn-Hilliard model using the stabilized-invariant energy quadratization (S-IEQ) approach. *omputer Physics Communications*, 238:36–49, 2019.
- [52] J. Yan, C.-W. Shu. Local discontinuous Galerkin methods for partial differential equations with higher order derivatives. *J. Sci. Comput.*, 17(1):24–47, 2002.
- [53] X. Yang. Linear, first and second order and unconditionally energy stable numerical schemes for the phase field model of homopolymer blends. *J. Comput. Phys.*, 302:509–523, 2016.
- [54] J. Zhao, X. Yang, Y. Gong, X. Zhao, J. Li, X. Yang and Q. Wang. Linear, second order and unconditionally energy stable schemes for the viscous Cahn-Hilliard equation with hyperbolic relaxation. *J. Comput. Appl. Math.*, 343:80–97, 2018.

‡ IOWA STATE UNIVERSITY, DEPARTMENT OF MATHEMATICS, AMES, IA 50011

Email address: `hliu@iastate.edu`

§ WAYNE STATE UNIVERSITY, DEPARTMENT OF MATHEMATICS, DETROIT, MI 48202

Email address: `pyin@wayne.edu`